Volume 44 | Number 36 | 28 September 2015 | Pages 15727–16178

Dalton Transactions

An international journal of inorganic chemistry

www.rsc.org/dalton

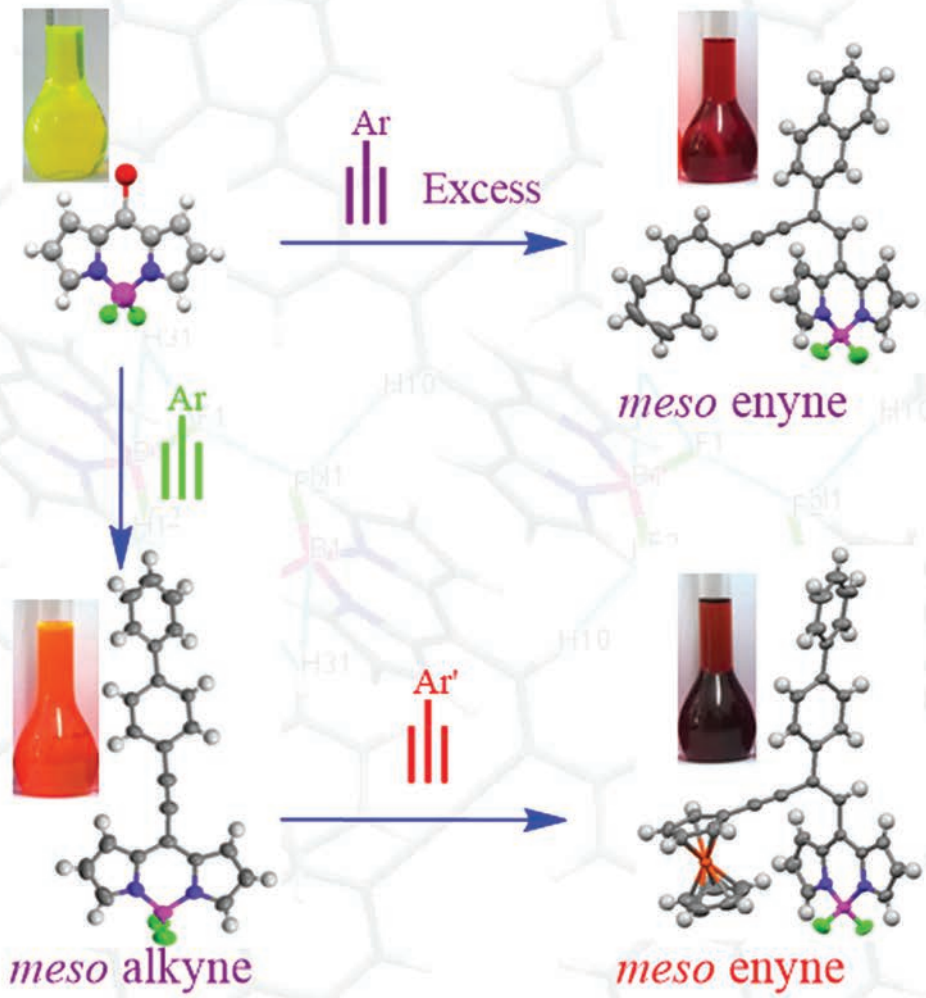

ISSN 1477-9226

ROYAL SOCIETY OF CHEMISTRY

PAPER

Rajneesh Misra *et al.*

Meso enyne substituted BODIPYs: synthesis, structure and properties

Dalton Transactions

PAPER

View Article Online
View Journal | View Issue

Cite this: *Dalton Trans.*, 2015, **44**, 15803

Meso enyne substituted BODIPYs: synthesis, structure and properties†

Bhausaheb Dhokale, Thaksen Jadhav, Shaikh M. Mobin and Rajneesh Misra*

Received 7th February 2015,
Accepted 13th March 2015

DOI: 10.1039/c5dt00565e

www.rsc.org/dalton

We report the synthesis of *meso* enyne substituted BODIPYs by the reaction of 8-chloro BODIPY with terminal alkynes under Sonogashira coupling conditions, and by Pd–Cu catalyzed hydroalkynylation reaction of terminal alkynes, across the –C≡C– bond of *meso* alkynylated BODIPYs. The scope of reaction was explored by reacting different *meso* alkynylated BODIPYs with various terminal alkynes, which results in *meso* enyne substituted BODIPYs with different substituents. The *meso* enyne substituted BODIPYs show blue shifted absorption and red shifted emission with large Stokes shift compared to *meso* alkynylated BODIPYs. The single crystal structures of BODIPYs **2a**, **3b**, **4a** and **2d** are reported. Their packing diagram exhibits extensive intermolecular C–H···π, C–H···F hydrogen bonding and π···π stacking interactions, leading to 1D supramolecular frameworks extending into the complex 3D structural frameworks.

Introduction

The BODIPY fluorophore outdistances itself from contemporary fluorophores, due to its unique photophysical properties such as strong absorption with high molar extinction coefficient and high fluorescence quantum yield.[1] The BODIPY dyes have been explored for variety of applications such as ion sensing, non-linear optics, organic photovoltaics, photodynamic therapy and bio-medical imaging.[2] The photonic properties of the BODIPY fluorophore can be tuned by introducing appropriate functionalities at α, β and *meso* positions or by ring-fusion.[3] The *meso* alkynylated BODIPYs exhibit red shifted absorption compared with α and β-alkynylated BODIPYs, but their absorption is blue shifted compared with α-alkynylated benzo-fused BODIPYs.[4]

Our group is involved in the design and synthesis of donor substituted, β and *meso* functionalized BODIPYs for optoelectronic applications.[5] Recently we reported the synthesis of *meso* enamine substituted BODIPYs by a catalyst free oxidation of *tert*-amines and cross coupling with 8-chloro BODIPY.[6]

Enynes are important building blocks in synthetic chemistry, and have been explored in organic electronics.[7] The literature reveals formation of enynes as a side product in the Sonogashira coupling reaction of certain aryl halides with terminal alkynes.[8] There are few reports, where enynes were obtained as the major product.[9] Tremendous efforts have been devoted for the selective synthesis of *E* or *Z* enynes by metal catalyzed alkyne dimerization.[10]

Herein we report the synthesis of *meso* enyne substituted BODIPYs by reacting excess terminal alkynes with 8-chloro BODIPY under Sonogashira coupling conditions (Method A), and by the Pd–Cu catalyzed hydroalkynylation reaction of terminal alkynes across the –C≡C– bond of *meso* alkynylated BODIPY (Method B) and their structural, photophysical and electrochemical properties. The reaction methodology furnishes, *meso* enyne substituted BODIPYs in good yields with two different substituents at a time. The methodology involves Pd–Cu catalyzed –C≡C– bond activation and new C–C bond formation.

Results and discussion

The reaction of 8-chloro BODIPY **1**, with excess terminal alkynes **a** and **b** under Sonogashira coupling conditions resulted in BODIPYs **2a** and **2b** as major products in 58% and 57% yields along with minor products **3a** and **3b** in 20% and 21% yields respectively (Method A; Scheme 1).

The isolated *meso* alkynylated BODIPYs **2a** and **2b** were subjected to Pd–Cu catalyzed hydroalkynylation reaction with alkynes **a** and **b**, which resulted in *meso* enyne substituted BODIPYs **3a** and **3b** in 60% and 62% yield respectively (Method B; Scheme 1). The reaction works well in different solvents like tetrahydrofuran, toluene and dichloromethane, but the presence of both $Pd(PPh_3)_2Cl_2$ and CuI catalysts is essential for the reaction.

Department of Chemistry, Indian Institute of Technology, Indore 452 017, India. E-mail: rajneeshmisra@iiti.ac.in; Fax: +91 731 2361 482

†Electronic supplementary information (ESI) available: Photophysical and electrochemical characterization data, copies of HRMS, ^{1}H, ^{13}C, ^{11}B and ^{19}B NMR spectra. CCDC 1018403–1018405 for **2a**, **3b** and **4a** respectively and 1041639 for **2d**. For ESI and crystallographic data in CIF or other electronic format see DOI: 10.1039/c5dt00565e

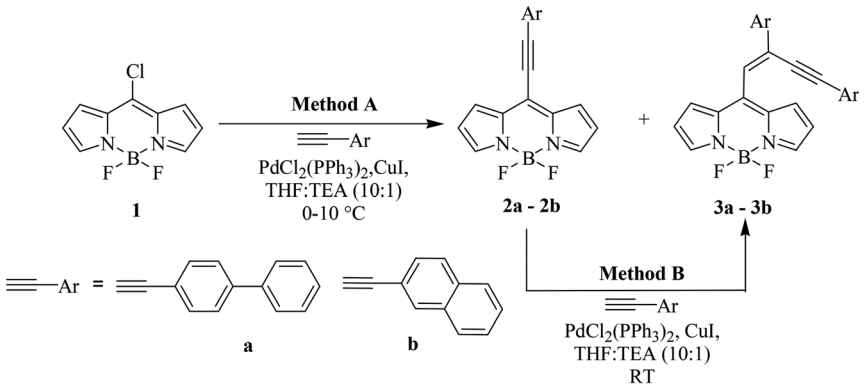

Scheme 1 Synthesis of *meso* ethynyl and enyne substituted BODIPYs **2a**, **2b** and **3a**, **3b**.

The scope of the reaction was explored to incorporate two different substituents into the BODIPY. The *meso* alkynylated BODIPYs **2a–2c** were subjected to Pd–Cu catalyzed hydroalkynylation reaction with ethynyl ferrocene (Scheme 2), which resulted in *meso* enyne substituted BODIPYs **4a**, **4b** and **4c** in 61%, 60% and 58% yields respectively.

The scope of the reaction was further explored for the Stille coupling. We tried the Stille reaction of (phenylethynyl)tributylstannane with the 8-chloro BODIPY. The reaction resulted only in *meso* alkynylated BODIPY **2d** in 80% yield (Scheme 3). Even the use of excess (phenylethynyl)tributylstannane in the Stille reaction resulted only in BODIPY **2d**.[11]

The plausible mechanism for the Pd–Cu catalyzed hydroalkynylation reaction across the –C≡C– of *meso* alkynylated BODIPYs is displayed in Scheme 4. The coordination of $Pd^{[0]}$ species with the –C≡C– bond of *meso* alkynylated BODIPY results in π-complex **A**. The activation of the terminal alkyne by Cu results in σ-complex **B**. The combination of **A** and **B** leads to the intermediate **C**, which further transforms into the *meso* alkynylated BODIPY.[12]

The BODIPYs were well characterized by ^{1}H NMR, ^{13}C NMR and HRMS techniques. The BODIPYs **2a**, **3b**, **4a** and **2d** were also characterized by single crystal X-ray crystallography.

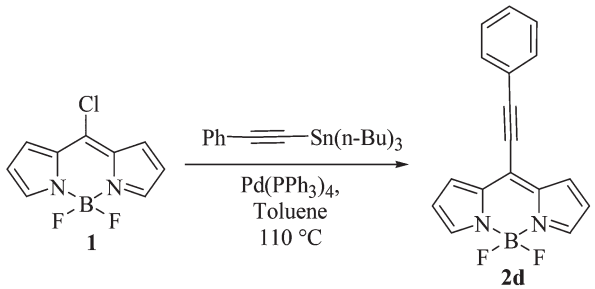

Scheme 3 Synthesis of BODIPY **2d** by the Stille reaction.

Photophysical properties

The electronic absorption and emission spectra of the BODIPYs **1–4** were recorded in toluene (Fig. 1 and S1–S3; ESI†) and the corresponding data are displayed in Table 1. The color variations in the BODIPY solution are shown in Fig. 2. The *meso* alkynylated BODIPYs **2a–2c** exhibit absorption bands at ~548 nm. The electronic absorption spectrum of *meso* enyne substituted BODIPYs **3a** and **3b** exhibits a blue shift of ~34 nm compared to the *meso* alkynylated BODIPYs **2a–2c** due to the

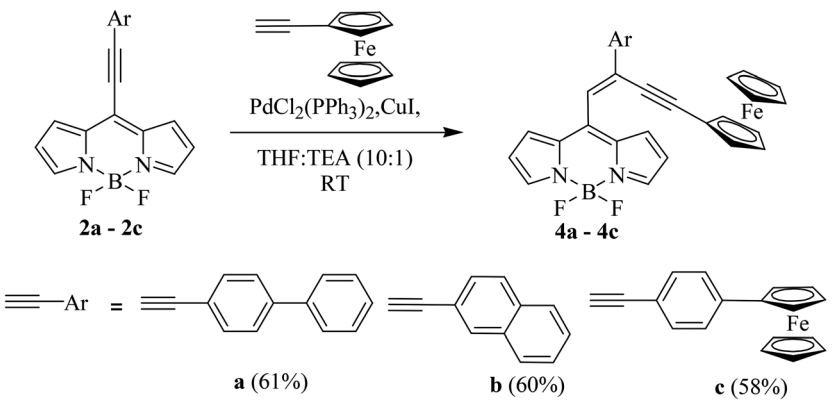

Scheme 2 Synthesis of *meso* ferrocenyl enyne substituted BODIPYs **4a–4c** (isolated yields in brackets).

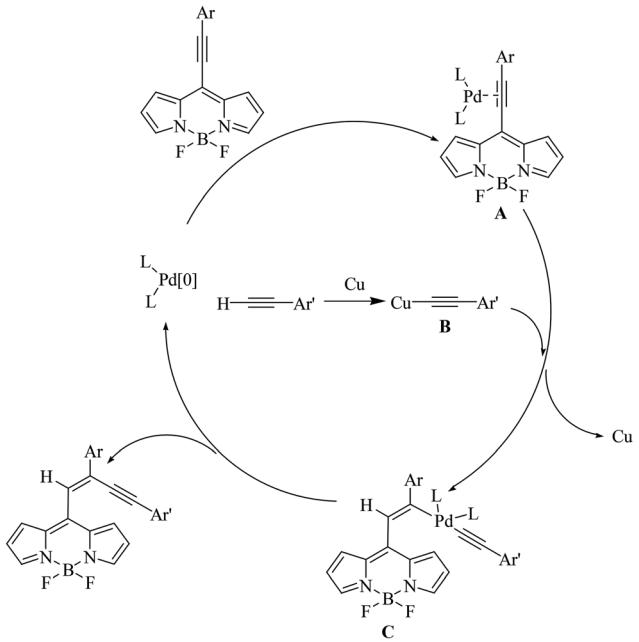

Scheme 4 Plausible reaction mechanism.

loss of planarity between the enyne substituent and BODIPY (torsional angle from the crystal structure 50.60°).

The ferrocenyl enyne substituted BODIPYs **4a–4c** exhibit a blue shift of ~38 nm, which suggests that incorporation of a bulkier alkyne (ethynyl ferrocene) disturbs the planarity more than the BODIPYs **3a–3c** (torsional angle from the crystal structure 58.41°).

The *meso* alkynylated BODIPYs **2a** and **2b** exhibit a sharp emission band at ~566 nm whereas, the *meso* enyne substituted BODIPYs **3a** and **3b** exhibit an ~8 nm red shifted broad emission band with lower quantum yield. (Fig. 1 (b) and S3 (ESI†); Table 1). The decrease in fluorescence quantum yield

Table 1 Photophysical properties of BODIPYs **2–4**

BODIPY	λ_{max} (nm)	$\varepsilon \times 10^4$ [a] (M^{-1} cm^{-1})	λ_{em} [b] (nm)	Stokes shift (cm^{-1})	ϕ_F [c]
2a	548	4.1	566	580	0.50
2b	549	4.2	567	578	0.43
3a	515	3.4	575	2026	0.05
3b	515	3.6	575	2026	0.04
4a	510	3.4	572	1940	0.0001
4b	510	3.5	568	2095	0.0004
4c	511	3.7	—[d]	—	—

[a] Recorded at λ_{max}. [b] Excited at λ_{max}. [c] Determined by using rhodamine 6G as the standard (ϕ = 0.88, in ethanol). [d] BODIPYs are non-emissive in nature.

can be attributed to the dissipation of the excited state energy by increased molecular rotations.[13] The BODIPYs bearing ferrocenyl units (**4a–4c**) are poorly emissive in nature due to the fast non-radiative deactivation of the excited state with intramolecular charge transfer from the donor ferrocenyl unit to the acceptor BODIPY moiety.[14]

The *meso* alkynylated BODIPYs **2a**, **2b** and **2c** exhibit Stokes shifts of 500–600 cm^{-1}, whereas the *meso* enyne substituted BODIPYs **3a**, **3b**, **4a** and **4b** exhibit Stokes shifts of ~2000 cm^{-1}. The large Stokes shift of enyne substituted BODIPYs can be attributed to the higher differences in the excited state dipole moment and free molecular rotations.[13] The absorption and emission spectra of the BODIPYs were recorded in different solvents. The absorption spectra of BODIPYs **2–4** show blue shifts in polar solvents and red shifts in non-polar solvents (Fig. S4–S9†), which indicates the negative solvatochromic effect.

Electrochemical properties

The electrochemical properties of BODIPYs **2–4** were investigated by cyclic and differential pulse voltammetric (CV and

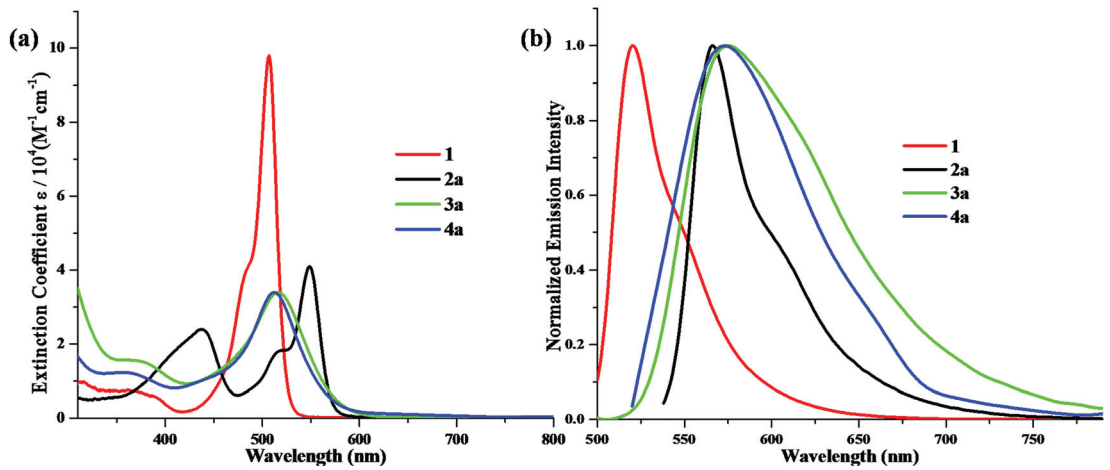

Fig. 1 (a) Electronic absorption spectra and (b) normalized emission spectra of BODIPYs **1**, **2a**, **3a** and **4a** in toluene at a concentration of 0.1 optical densities at λ_{max}.

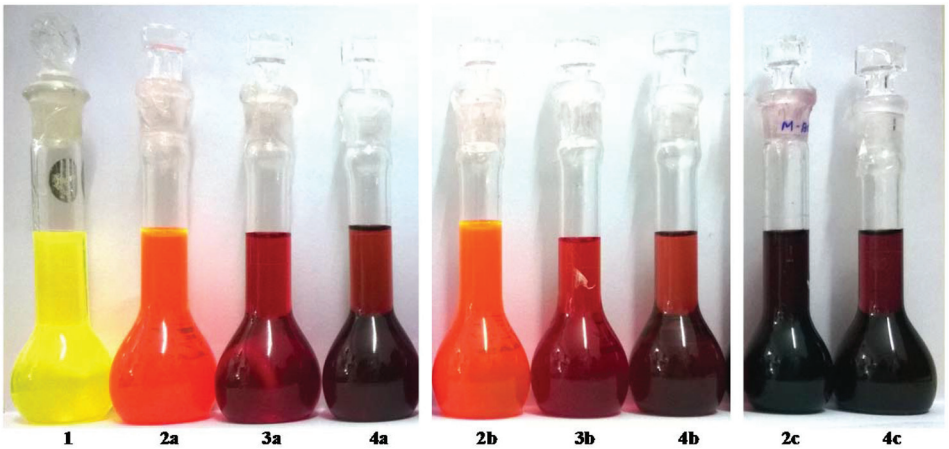

Fig. 2 BODIPYs **1–4** in toluene at 10^{-4} M concentration.

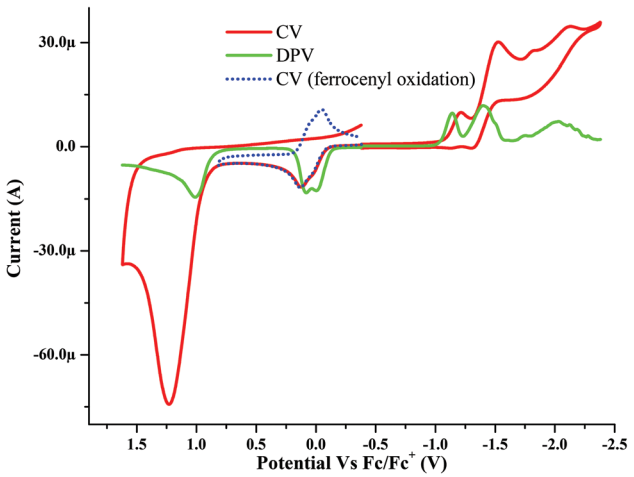

Fig. 3 Overlaid CV and DPV plots of the *meso* enyne substituted BODIPY **4c** bearing two ferrocenyl units in different environments.

DPV) techniques in a 0.1 M solution of Bu_4NPF_6 in dichloromethane at 100 mV s^{-1} scan rate, *versus* Fc/Fc^+ (Fig. 3 and S10–S13†). The electrochemical data are displayed in Table 2. The redox waves of the BODIPY origin are irreversible, whereas the ferrocenyl oxidation waves are reversible in nature (dotted blue line; Fig. 3).

The first reduction potential follows the order **2a** > **3a** > **4a** (Table 2), indicating better delocalization of donor electrons onto the BODIPY moiety in *meso* enyne substituted BODIPYs compared to *meso* alkynylated BODIPYs. The harder reduction of BODIPY **4** compared to BODIPY **3** indicates a better electron donating ability of ferrocene than biphenyl and naphthalene moieties.

The BODIPY **4c** exhibits two merging oxidation waves in CV and DPV at 0.08 V and 0.00 V, corresponding to the oxidation of the ferrocenyl moiety attached to the triple bond and the phenyl ring respectively.

Theoretical calculations

Computational calculation was performed using density functional theory (DFT), and the frontier molecular orbitals (FMOs) of the BODIPYs **2–4** are displayed in Fig. 4 and S22 (ESI†). The LUMO in BODIPYs **2a**, **3a** and **4a** are localized on the BODIPY core, which indicates the strong acceptor nature of BODIPY. The HOMO in **2a** is distributed on BODIPY and in **3a** on

Table 2 The electrochemical properties of the BODIPYs **2–4**[a]

BODIPY	E^2 Oxid.[b] (BODIPY)	E^1 Oxid.[b] (BODIPY)	E^1 Oxid. (Fc)	E^1 Red.[b] (BODIPY)	E^2 Red.[b] (BODIPY)
2a	1.35	1.10	—	−0.98	−1.35
2b	1.28	1.07	—	−0.99	−1.28
3a	1.41	1.01	—	−1.04	−1.36
3b	1.33	0.97	—	−1.08	−1.41
4a	—	1.16	0.10	−1.12	−1.40
4b	—	1.17	0.08	−1.13	−1.43
4c	—	1.01	0.00 (Phenyl Fc) 0.08 (Ethynyl Fc)	−1.14	−1.40

[a] The electrochemical analysis was performed in a 0.1 M solution of Bu_4NPF_6 in dichloromethane at 100 mV s^{-1} scan rate, *versus* Fc/Fc^+. [b] Irreversible wave.

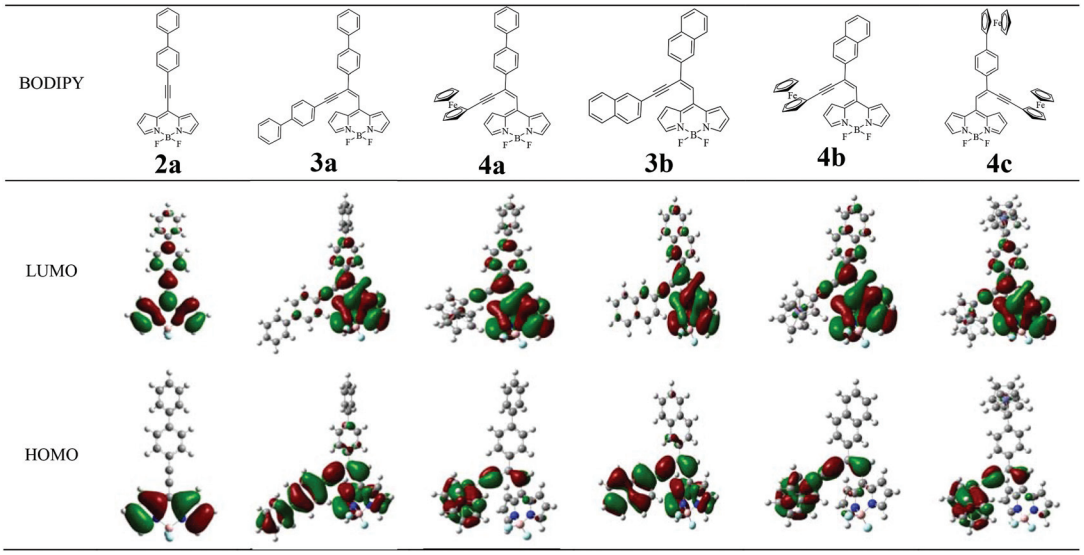

Fig. 4 Frontier molecular orbital plots of BODIPYs **2–4**, calculated at the B3LYP/6-31G* level for C, N, B, F, H, and the Lanl2DZ level for Fe.

BODIPY as well as on the ethynyl biphenyl moiety, indicating better electronic distribution. The HOMO in BODIPY **4a** is localized on the ferrocenyl part only due to the stronger electron donating ability of ethynyl ferrocene than ethynyl biphenyl. The overall distribution of HOMO on the aryl moiety and LUMO on BODIPY reflects the strong donor acceptor interactions in *meso* enyne substituted BODIPYs.

Crystal structure

Single crystals of the BODIPYs **2a**, **3b**, **4a** and **2d** were obtained by slow evaporation of their dichloromethane–hexane solution at room temperature. The BODIPY **2a** crystallizes in the monoclinic $C2/c$ space group, **3b** and **4a** crystallizes in the triclinic $P\bar{1}$ space group, whereas the BODIPY **2d** crystallizes in the monoclinic $P2_1/c$ space group. The crystal structure and data refinement parameters are displayed in Table S2 (ESI†). The crystal structures reveal that the *meso* enyne substituted BODIPYs were obtained only in (*E*) conformation. The highly planar BODIPY core in *meso* alkynylated BODIPYs maintains planarity in *meso* alkynylated BODIPYs also (Fig. 5).

The comparison of selected bond lengths and bond angles of the crystal structure is shown in Fig. S20 and S21 (ESI†) respectively. The *meso* substituent and the BODIPY core are planar in *meso* alkynylated BODIPYs, and non-planar in *meso* enyne substituted BODIPYs. The higher torsional angle between the BODIPY plane and the *meso* enyne substituent in BODIPY **4a** than BODIPY **3b**, suggests the bulky nature of the

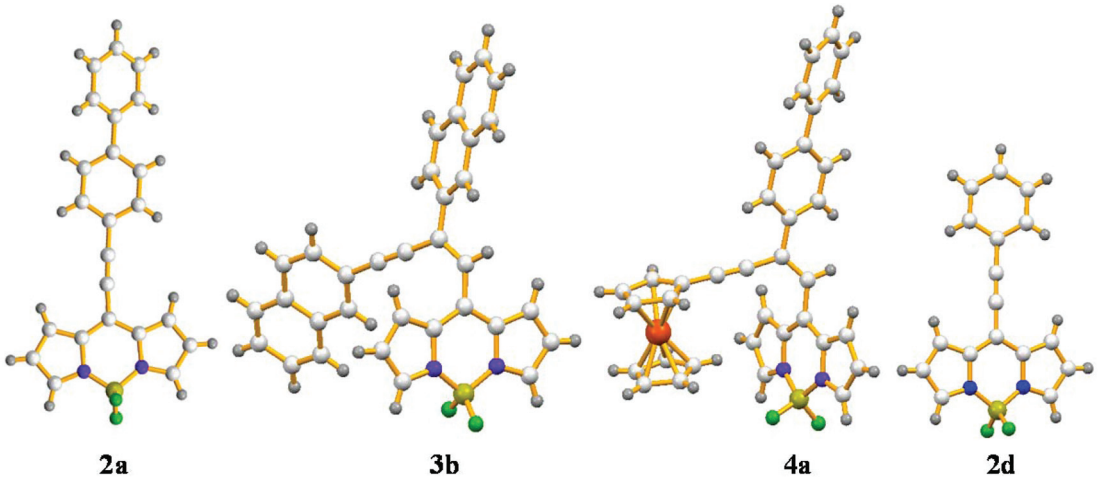

Fig. 5 Single crystal structures of BODIPYs **2a**, **3b**, **4a** and **2d** (BODIPY **2a**: only molecule B is shown from the asymmetric unit; details in Fig. S14; ESI†).

Table 3 Distances and angles of intermolecular interactions in the crystal structures of BODIPYs **2a**, **3b**, **4a** and **2d**

Sr. no.	Interaction	Distance (Å)	Angle (°)
BODIPY **2a**			
1	C(1)–H(1)···F(1)	2.504	147.10
2	C(3)–H(3)···F(3)	2.588	172.52
3	C(13)–H(13)···F(3)	2.527	147.56
4	C(59)–H(59)···F(4)	2.402	158.47
5	C(32)–H(32)···F(5)	2.413	155.87
6	C(32)–H(32)···F(6)	2.597	150.25
7	C(16)–H(16)···π (Pyrrolic)	2.481	
8	C(17)–H(17)···π (Pyrrolic)	3.277	
9	C(31)–H(31)···π (Pyrrolic)	3.093	
10	C(25)–H(25)···π (Pyrrolic)	2.892	
11	C(46)–H(46)···π (Phenyl)	3.606	
BODIPY **3b**			
1	C(31)–H(31)···F(1)	2.638	145.99
2	C(1)–H(1)···F(1)	2.354	164.33
3	C(10)–H(10)···F(2)	2.493	165.23
4	C(3)–H(3)···π (Naph)	3.183	
5	C(28)–H(28)···π (Naph)	2.733	
BODIPY **4a**			
1	C(9)–H(9)···F(1)	2.664	161.46
2	C(9)–H(9)···F(2)	2.645	147.39
3	C(10)–H(10)···F(2)	2.324	153.72
4	C(1)–H(1)···π (Fc)	3.183	
5	C(7)–H(7)···π (Fc)	3.395	
6	C(28)–H(28)···π (Phenyl)	3.271	
7	C(23)–H(23)···π (Fc)	2.731	
BODIPY **2d**			
1	C(1)–H(1)···F(1)	2.397	160.15
2	C(8)–H(8)···F(2)	2.570	153.85
3	C(17)–H(17)···F(2)	2.541	152.86
4	C(13)–H(13)··· π (Pyrrolic)	3.198	
5	π (Pyrrolic)···π (Pyrrolic)		

ferrocenyl moiety than the naphthalene moiety, which supports the higher blue shift in the absorption spectra of **4a** and **4b** than **3a** and **3b**.

The close packing in the crystal structures of BODIPYs **2a**, **3b**, **4a** and **2d** exhibits marvelous supramolecular frameworks. The distances and angles of the supramolecular interactions in the crystals are shown in Table 3.

The crystal structure of BODIPY **2a** contains three molecules (A, B and C) in an asymmetric unit. These three molecules slightly differ in bond lengths and angles. The C(46)–H(46)···π (phenyl) interaction connects molecule B and C whereas the (13)–H(13)···F(3) and C(3)–H(3)···F(3) interactions connect molecules B and A. The molecules B and C form a chain along the *c*-axis with molecule A hanging above the chain with C(32)–H(32)···F(6) and C(32)–H(32)···F(5) interactions. The two chains are arranged in an antiparallel fashion *via* π···π stacking interactions between two pyrrolic rings of molecule C. The set of two antiparallel chains further grows into a complex 3D framework *via* C(1)–H(1)···F(1), C(59)–H(59)···F(4), C(16)–H(16)···π (pyrrolic), C(17)–H(17)···π (pyrrolic) and C(31)–H(31)···π (pyrrolic) interactions (Fig. 6).

In the packing diagram of BODIPY **3b**, the two molecules form a dimeric structure in a head to head sliding manner *via* two mutual C(10)–H(10)···F(2) interactions. These dimers connect to one-another diagonally to form a 1D chain along the *a*-axis *via* C(31)–H(31)···F(1) and C(1)–H(1)···F(1) interactions (Fig. 7(a)). These one dimensional chains connect to another chains laterally *via* C(3)–H(3)···π and C(28)–H(28)···π interactions along the *b* and *c* axis respectively to form a complex 3D framework (Fig. 7(b)).

In the crystal structure packing of BODIPY **4a**, four mutual hydrogen bonding C(9)–H(9)···F(1) and C(9)–H(9)···F(2) interactions form a head to head pair. This pair connects to the neighboring pair *via* C(7)–H(7)···π (Fc) and C(28)–H(28)···π (phenyl) interactions forming a hydrogen bonded tetramer (Fig. 8). This tetramer further grows above and below *via* two mutual interactions C(10)–H(10)···F(2) to form a chain of tetramers, which further form a thick sheet *via* C(23)–H(23)···π (Fc) interactions (Fig. S19 (ESI†)).

In the crystal structure packing of BODIPY **2d** the head to tail π···π stacking between two BODIPY frameworks forms a dimeric structure which is stabilized by C(17)–H(17)···F(2) interactions. These dimeric structures extend into a 1D chain *via* interactions C(13)–H(13)···π (pyrrolic). The 1D chain further extends to a complex 3D framework *via* interactions C(8)–H(8)···F(2) and C(1)–H(1)···F(1) (Fig. 9).

Conclusions

We have developed a straightforward route for the synthesis of *meso* enyne substituted BODIPYs with two different substituents. The *meso* enyne substituted BODIPYs exhibit large Stokes shifts, compared to the *meso* alkynylated BODIPYs. The electrochemical properties and theoretical calculations reveal strong donor–acceptor interactions between the enyne substituent and the BODIPY. *Meso* enyne substituted BODIPYs with two different substituents are potential candidates for optoelectronic applications. This methodology would enable the rapid construction of a library of multi-substituted BODIPYs. The synthesis of new enyne substituted BODIPYs and their optoelectronic applications are ongoing in our group.

Experimental section

Chemicals were used as received unless otherwise indicated. All oxygen or moisture sensitive reactions were performed under a nitrogen/argon atmosphere using standard Schlenk methods. Triethylamine (TEA) was received from a commercial source and distilled in KOH prior to use. ^{1}H NMR (400 MHz), and ^{13}C NMR (100 MHz) spectra were recorded on a Bruker Avance (III) 400 MHz instrument using $CDCl_3$ as the solvent. ^{1}H NMR chemical shifts are reported in parts per million (ppm) relative to the solvent residual peak ($CDCl_3$, 7.26 ppm). Multiplicities are given as: s (singlet), d (doublet), t (triplet), q (quartet), dd (doublet of doublets), m (multiplet), and the coupling constants, *J*, are given in Hz. ^{13}C NMR chemical

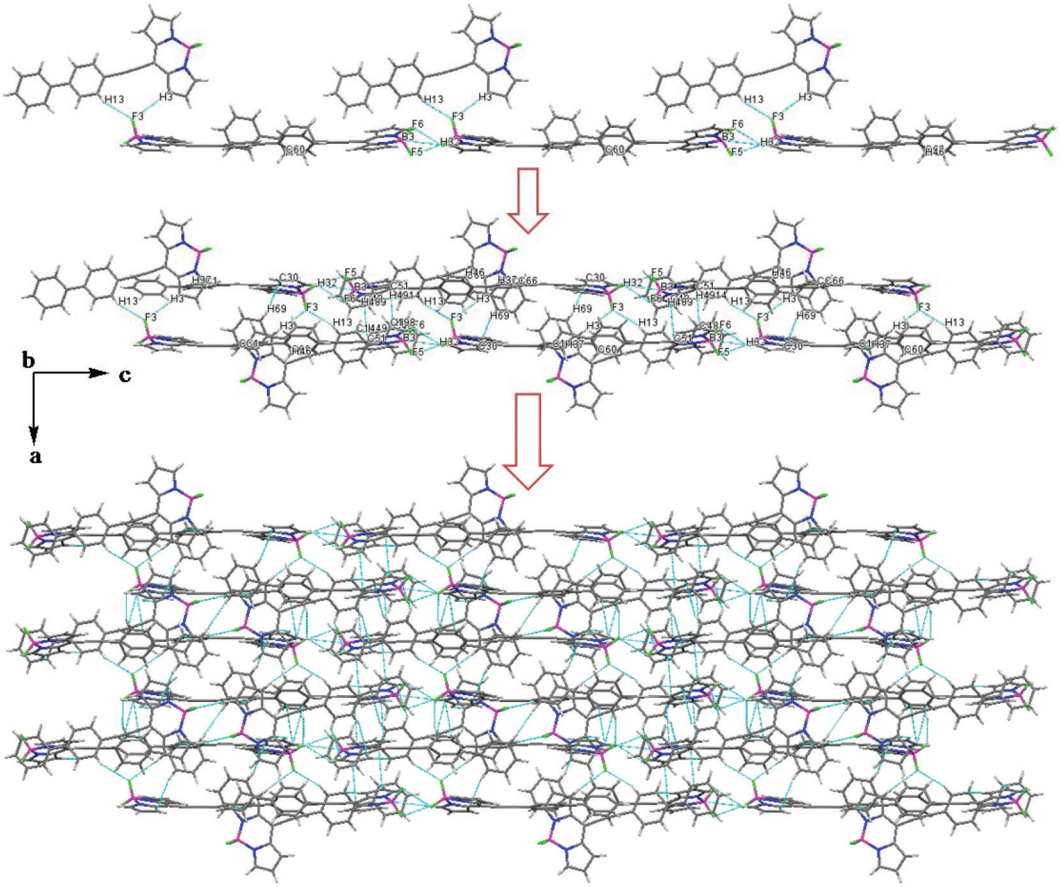

Fig. 6 Crystal structure packing of BODIPY **2a**.

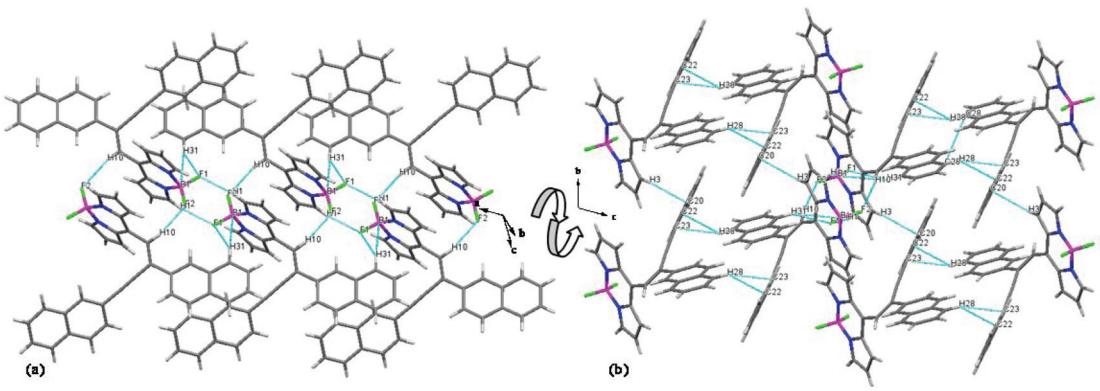

Fig. 7 Crystal structure packing of BODIPY **3b**.

shifts are reported relative to the solvent residual peak ($CDCl_3$, 77.36 ppm). HRMS were recorded on a Bruker-Daltonics micrOTOF-Q II mass spectrometer. UV-visible absorption spectra of all compounds were recorded on a Cary-100 Bio UV-visible spectrophotometer and fluorescence spectra were recorded on Horiba Jobin Yvon Fluoromax 4P spectrophotometers in toluene at a concentration of 0.1 optical densities at λ_{max}. The voltammograms were recorded on a CHI620D electrochemical analyzer in dichloromethane solvent and 0.1 M $TBAF_6$ as the supporting electrolyte. The electrodes used were glassy carbon as a working electrode, Pt wire as a counter electrode and the saturated calomel electrode as a reference electrode. The potentials were referenced against Fc/Fc^+ as per IUPAC guidelines.[12]

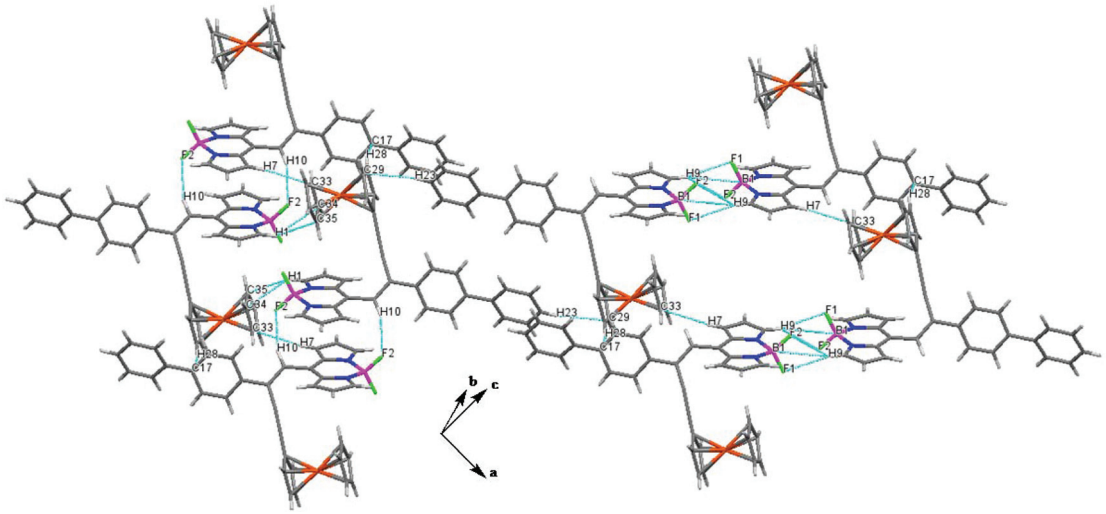

Fig. 8 Crystal structure packing of BODIPY **4a**.

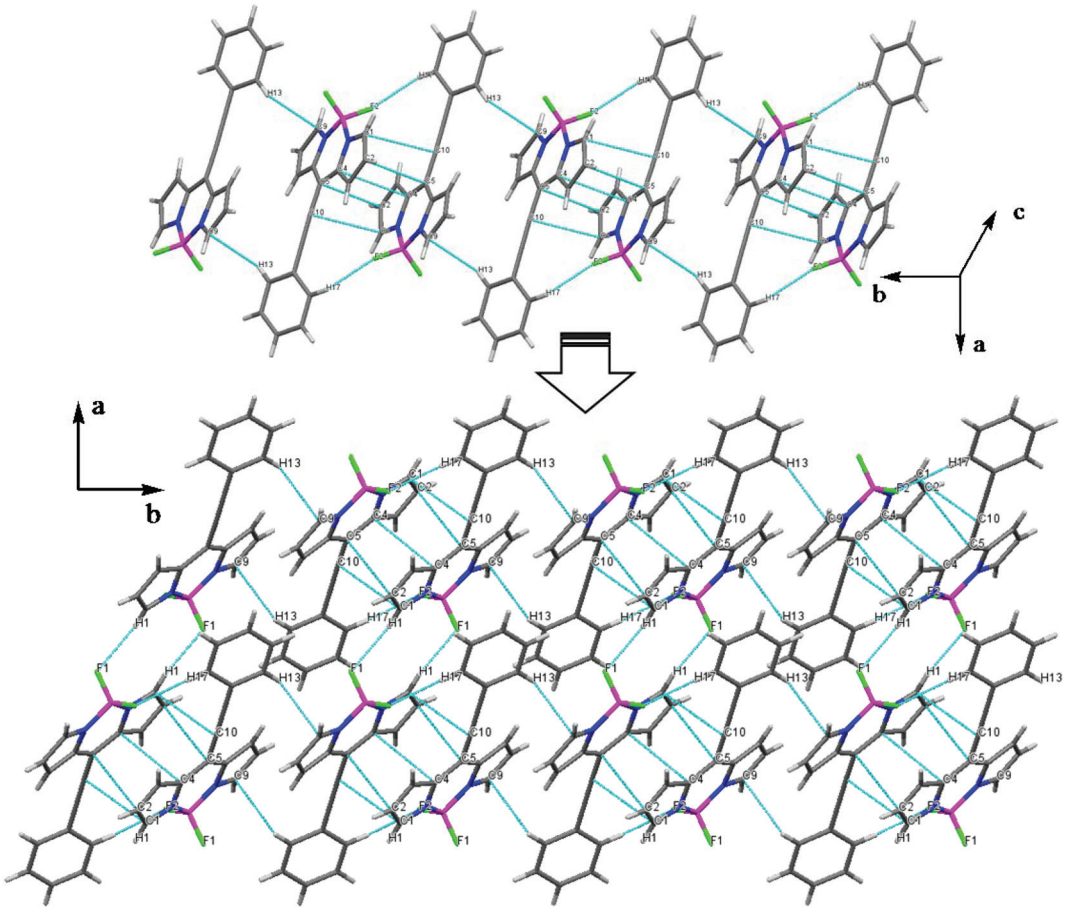

Fig. 9 Crystal structure packing of BODIPY **2d**.

Generalized synthetic procedure for BODIPYs 2a, 2b, 3a and 3b (Method A)

8-Chloro BODIPY **1** (100 mg, 0.44 mmol), and the corresponding arylethynes (**a** or **b**) (0.66 mmol) were dissolved in THF–triethylamine (10 : 1,v/v; 15 ml), and the mixture was cooled to 0 °C using an ice bath. The reaction mixture was purged with argon, and $Pd(PPh_3)_2Cl_2$ (15 mg, 5 mol%), and CuI (8.3 mg, 10 mol%) were added, followed by stirring at 0 °C for 30 min. The reaction mixture was brought to room temperature and further stirred for 4 h. After complete conversion of the starting aryl alkyne **a**/**b**, the reaction mixture was evaporated to dryness, and the crude product was dissolved in CH_2Cl_2, chromatographed on silica (2 : 1; hexanes–CH_2Cl_2) to get **2a**/**2b** and **3a**/**3b**. The isolated products from column chromatography were recrystallized from the chloroform–hexane (1 : 3) mixture as a crystalline solid.

Generalized synthetic procedure for BODIPYs 3a, 3b, 4a, 4b and 4c (Method B)

Meso alkynylated BODIPY (**2a**, **2b** or **2c**) (0.30 mmol) and aryl alkyne (ethynyl biphenyl, ethynyl naphthalene or ethynyl ferrocene) (0.30 mmol) were dissolved in THF–triethylamine (10 : 1, v/v; 15 ml). The reaction mixture was purged with argon, and $Pd(PPh_3)_2Cl_2$ (10.0 mg, 5 mol%), and CuI (6.7 mg, 10 mol%) were added, followed by stirring at room temperature for 10 h. After completion of the reaction, the reaction mixture was evaporated to dryness, and the crude product was dissolved in CH_2Cl_2, chromatographed on silica (1 : 2; hexanes–CH_2Cl_2) to get **3a**, **3b**, **4a**, **4b** or **4c**. The isolated products from column chromatography were recrystallized from the chloroform–hexane (1 : 3) mixture as a crystalline solid.

Characterization data

3a. Red crystalline solid. Yield: **Method A** – 20% (48 mg); **Method B** – 60% (89 mg); ^{1}H NMR ($CDCl_3$, 400 MHz, ppm): δ 7.99–7.96 (m, 2H), 7.91 (bs, 2H), 7.76–7.73 (m, 2H), 7.69–7.66 (m, 2H), 7.58–7.55 (m, 2H), 7.53–7.50 (m, 3H), 7.48–7.45 (m, 4H), 7.44–7.41 (m, 2H), 7.40–7.34 (m, 2H), 7.33–7.30 (m, 2H), 6.55–7.53 (m, 2H); ^{13}C NMR ($CDCl_3$, 100 MHz, ppm): 144.0, 143.1, 142.8, 142.4, 140.4, 140.38, 136.4, 134.5, 133.3, 132.6, 130.1, 129.3, 129.2, 128.3, 128.2, 127.9, 127.8, 127.5, 127.4, 127.37, 125.4, 121.1, 118.3, 100.3, 87.4; ^{11}B NMR ($CDCl_3$, 128 MHz, ppm) 0.28 (t, J_{B-F} = 28.7 Hz); UV/vis (toluene): λ_{max} (ε [M^{-1} cm^{-1}]) 515 (3.38×10^4). HRMS (ESI-TOF) m/z = calculated for $C_{37}H_{25}BF_2N_2$ = 585.1717 $[M + K]^+$, measured 585.1720 $[M + K]^+$.

4a. Purple-red crystalline solid. Yield: 61% (96 mg);. ^{1}H NMR ($CDCl_3$, 400 MHz, ppm): δ 7.93–7.90 (m, 4H), 7.74–7.70 (m, 2H), 7.68–7.65 (m, 2H), 7.51–7.48 (m, 2H), 7.43–7.39 (m, 4H), 6.57–6.55 (m, 2H), 4.27 (t, 2H, J = 1.76 Hz), 4.23 (t, 2H, J = 1.76 Hz), 4.08 (s, 5H); ^{13}C NMR ($CDCl_3$, 100 MHz, ppm): 143.7, 143.6, 142.9, 140.4, 136.5, 134.9, 133.8, 130.5, 129.3, 128.2, 127.8, 127.75, 127.4, 123.7, 118.1, 101.0, 83.4, 72.1, 70.5, 70.0, 63.7; ^{11}B NMR ($CDCl_3$, 128 MHz, ppm) 0.29 (t, J_{B-F} = 29.5 Hz); UV/vis (toluene): λ_{max} (ε [M^{-1} cm^{-1}]) 510 (3.4×10^4). HRMS (ESI-TOF) m/z = calculated for $C_{35}H_{25}BF_2FeN_2$ = 578.1429 $[M]^+$, measured 578.1425 $[M]^+$.

3b. Red crystalline solid. Yield: **Method A** – 21% (46 mg); **Method B** – 62% (89 mg); ^{1}H NMR ($CDCl_3$, 400 MHz, ppm): δ 8.42 (s, 1H), 8.01–8.98 (m, 3H), 7.93–7.91 (m, 3H), 7.80–7.73 (m, 4H), 7.60–7.57 (m, 2H), 7.56 (s, 1H), 7.51–7.48 (m, 4H), 7.29–7.27 (m, 1H), 6.54–6.53 (m, 2H); ^{13}C NMR ($CDCl_3$, 100 MHz, ppm): 144.0, 143.0, 134.7, 134.6, 134.3, 133.8, 133.6, 133.5, 133.2, 132.8, 130.2, 129.1, 129.0, 128.5, 128.4, 128.3, 128.13, 128.1, 127.9, 127.7, 127.6, 127.3, 127.1, 126.1, 124.0, 119.6, 118.3, 101.0, 87.3; ^{11}B NMR ($CDCl_3$, 128 MHz, ppm) 0.34 (t, J_{B-F} = 29.5 Hz); UV/vis (toluene): λ_{max} (ε [M^{-1} cm^{-1}]) 515 (3.6×10^4). HRMS (ESI-TOF) m/z = calculated for $C_{33}H_{21}BF_2N_2$ = 517.1664 $[M + Na]^+$, measured 517.1651 $[M + Na]^+$.

4b. Purple crystalline solid. Yield: 60% (97 mg); ^{1}H NMR ($CDCl_3$, 400 MHz, ppm): δ 8.32 (s, 1H), 7.97–7.89 (m, 6H), 7.58–7.54 (m, 2H), 7.47 (s, 1H), 7.44 (d, 2H, J = 4 Hz), 6.57–6.56 (m, 2H), 4.30 (t, 2H, J = 1.76 Hz), 4.24 (t, 2H, J = 1.76 Hz), 4.09 (s, 5H); ^{13}C NMR ($CDCl_3$, 100 MHz, ppm): 143.8, 143.6, 134.9, 134.7, 134.2, 134.16, 133.5, 130.1, 129.1, 128.9, 128.1, 127.9, 127.6, 127.2, 124.3, 124.0, 118.2, 101.0, 83.39, 72.4, 70.9, 70.3, 53.8; ^{11}B NMR ($CDCl_3$, 128 MHz, ppm) 0.31 (t, J_{B-F} = 28.7 Hz); UV/vis (toluene): λ_{max} (ε [M^{-1} cm^{-1}]) 510 (3.5×10^4). HRMS (ESI-TOF) m/z = calculated for $C_{33}H_{23}BF_2FeN_2$ = 575.1170 $[M + Na]^+$, measured 575.1170 $[M + Na]^+$.

4c. Purple crystalline solid. Yield: 58% (84 mg); ^{1}H NMR ($CDCl_3$, 400 MHz, ppm): δ 7.92 (s, 2H), 7.78–7.75 (m, 2H), 7.58–7.56 (m, 2H), 7.44 (d, 2H, J = Hz), 7.37 (s, 1H), 6.56–6.54 (m, 2H), 4.73 (t, 2H, J = 2 Hz), 4.41 (t, 2H, J = 1.76 Hz), 4.27 (m, 2H), 4.23 (t, 2H, J = 1.76 Hz), 4.09–4.08 (m, 10 H); ^{13}C NMR ($CDCl_3$, 100 MHz, ppm): 143.9, 143.5, 142.2, 134.9, 134.7, 134.2, 132.2, 130.0, 127.4, 126.5, 122.8, 118.0, 84.3, 83.5, 72.1, 70.5, 70.2, 70.0, 69.9, 87.1, 63.8; UV/vis (toluene): λ_{max} (ε [M^{-1} cm^{-1}]) 511 (3.7×10^4). HRMS (ESI-TOF) m/z = calculated for $C_{39}H_{29}BF_2Fe_2N_2$ = 686.1093 $[M]^+$, measured 686.1091 $[M]^+$.

Synthesis of BODIPY 2d

8-Chloro-BODIPY **1** (100 mg, 0.44 mmol) was dissolved in toluene and purged with argon. The (phenylethynyl)tributylstannane reagent and $Pd(PPh_3)_4$ (25.5 mg, 5 mol%) were added, followed by reflux for 20 h under an argon atmosphere. After completion of the reaction, the reaction mixture was evaporated to dryness, and the crude product was dissolved in CH_2Cl_2, chromatographed on silica (1 : 2; hexanes–CH_2Cl_2) to get BODIPY **2d**. The isolated product from column chromatography was recrystallized by slow evaporation of dichloromethane–hexane solution.

Product-red crystalline solid. Yield: 80% (104 mg); ^{1}H NMR ($CDCl_3$, 400 MHz, ppm): δ 7.84 (s, 2H), 7.67 (d, 2H, J = 6.76 Hz), 7.55–7.45 (m, 3H), 7.41 (d, J = 4 Hz, 2H), 6.55 (d, J = 4 Hz, 2H); ^{13}C NMR ($CDCl_3$, 100 MHz, ppm): δ 143.6, 136.6, 132.8, 131.1, 129.2, 128.9, 127.3, 120.9, 118.4, 106.0, 84.1 ppm; HRMS (ESI-TOF) m/z = calculated for $C_{17}H_{11}BF_2N_2$ = 315.0879 $[M + Na]^+$, measured 315.0879 $[M + Na]^+$. Data in agreement with the literature.[3h]

Acknowledgements

We thank DST New Delhi for financial support. BD and TJ thank CSIR and UGC New Delhi for their fellowships. We thank SIC, IIT Indore.

References

1 (*a*) H. Lu, J. Mack, Y. Yang and Z. Shen, *Chem. Soc. Rev.*, 2014, **43**, 4778–4823; (*b*) A. Loudet and K. Burgess, *Chem. Rev.*, 2007, **107**, 4891–4932; (*c*) J. Han and K. Burgess, *Chem. Rev.*, 2010, **110**, 2709–2728.

2 (*a*) A. Hagfeldt, G. Boschloo, L. C. Sun, L. Kloo and H. Pettersson, *Chem. Rev.*, 2010, **110**, 6595–6663; (*b*) O. A. Bozdemir, R. Guliyev, O. Buyukcakir, S. Selcuk, S. Kolemen, G. Gulseren, T. Nalbantoglu, H. Boyaci and E. U. Akkaya, *J. Am. Chem. Soc.*, 2010, **132**, 8029; (*c*) W. Pang, X.-F. Zhang, J. Zhou, C. Yu, E. Hao and L. Jiao, *Chem. Commun.*, 2012, **48**, 5437–5439; (*d*) X.-F. Zhang and X. Yang, *J. Phys. Chem. B*, 2013, **117**, 9050–9055; (*e*) X.-F. Zhang and X. Yang, *J. Phys. Chem. B*, 2013, **117**, 5533–5539; (*f*) X.-F. Zhang, X. Yang, K. Niu and H. Geng, *J. Photochem. Photobiol., A*, 2014, **285**, 16–20.

3 (*a*) A. B. Nepomnyashchii and A. J. Bard, *Acc. Chem. Res.*, 2012, **45**, 1844–1853; (*b*) N. Boens, V. Leen and W. Dehaen, *Chem. Soc. Rev.*, 2012, **41**, 1130–1172; (*c*) A. Bessette and G. S. Hanan, *Chem. Soc. Rev.*, 2014, **43**, 3342–3405; (*d*) G. Ulrich, R. Ziessel and A. Harriman, *Angew. Chem.*, 2008, **120**, 1202–1219, (*Angew. Chem., Int. Ed.*, 2008, **47**, 1184–1201); (*e*) A. Wakamiya, T. Murakami and S. Yamaguchi, *Chem. Sci.*, 2013, **4**, 1002; (*f*) M. Wada, S. Ito, H. Uno, T. Murashima, N. Ono, T. Urano and Y. Urano, *Tetrahedron Lett.*, 2001, **42**, 6711; (*g*) Z. Shen, H. Rohr, K. Rurack, H. Uno, M. Spieles, B. Schulz, G. Reck and N. Ono, *Chem. – Eur. J.*, 2004, **10**, 4853; (*h*) C. Yu, Y. Xu, L. Jiao, J. Zhou, Z. Wang and E. Hao, *Chem. – Eur. J.*, 2012, **18**, 6437; (*i*) M. Nakamura, H. Tahara, K. Takahashi, T. Nagata, H. Uoyama, D. Kuzuhara, S. Mori, T. Okujima, H. Yamada and H. Uno, *Org. Biomol. Chem.*, 2012, **10**, 6840.

4 (*a*) R. Misra, B. Dhokale, T. Jadhav and S. M. Mobin, *Dalton Trans.*, 2014, **43**, 4854; (*b*) X. Yang, X.-F. Zhang, X. Lu, C. Yu and L. Jiao, *J. Photochem. Photobiol., A*, 2015, **297**, 39–44.

5 (*a*) B. Dhokale, P. Gautam, S. M. Mobin and R. Misra, *Dalton Trans.*, 2013, **42**, 1512–1518; (*b*) P. Gautam, B. Dhokale, S. M. Mobin and R. Misra, *RSC Adv.*, 2012, **2**, 12105–12107; (*c*) R. Misra, B. Dhokale, T. Jadhav and S. M. Mobin, *Dalton Trans.*, 2014, **43**, 4854; (*d*) R. Misra, B. Dhokale, T. Jadhav and S. M. Mobin, *Organometallics*, 2014, **33**, 1867–1877; (*e*) R. Misra, B. Dhokale, T. Jadhav and S. M. Mobin, *New J. Chem.*, 2014, **38**, 3579–3585; (*f*) R. Misra, T. Jadhav, B. Dhokale, P. Gautam, R. Sharma, R. Maragani and S. M. Mobin, *Dalton Trans.*, 2014, **43**, 13076–13086.

6 B. Dhokale, T. Jadhav, S. M. Mobin and R. Misra, *Chem. Commun.*, 2014, **50**, 9119–9121.

7 Y. Liu, M. Nishiura, Y. Wang and Z. Hou, *J. Am. Chem. Soc.*, 2006, **128**, 5592–5593.

8 (*a*) A. Carpita and A. Ribecai, *Tetrahedron Lett.*, 2009, **50**, 204–207; (*b*) J. H. Olivier, F. Camerel, R. Ziessel, P. Retailleau, J. Amadou and C. Pham-Huu, *New J. Chem.*, 2008, **32**, 920–924; (*c*) L. Djakovitch and P. Rollet, *Adv. Synth. Catal.*, 2004, **346**, 1782–1792.

9 (*a*) P. Arsenyan, K. Rubina, J. Vasiljeva and S. Belyakov, *Tetrahedron Lett.*, 2013, **54**, 6524–6528; (*b*) M. Pal, R. Dakarapu, K. Parasuraman, V. Subramanian and K. R. Yeleswarapu, *J. Org. Chem.*, 2005, **70**, 7179–7187; (*c*) Y.-J. Chen, G.-H. Lee, S.-M. Peng and C. Y. Yeh, *Tetrahedron Lett.*, 2005, **46**, 1541–1544; Corrigendum: *Tetrahedron Lett.*, 2005, **46**, 3265; (*d*) J. J. Gonzalez, A. Francesch, D. J. Cardenas and A. M. Echavarren, *J. Org. Chem.*, 1998, **63**, 2854–2857; (*e*) I. G. Stara, I. Stary, A. Kollarovic, E. Teply, D. Saman and P. Fiedler, *Tetrahedron*, 1998, **54**, 11209–11234; (*f*) Y. Liu, S. Jin, Z. Wang, L. Song and Y. Hu, *Org. Lett.*, 2014, **16**, 3524–3527.

10 (*a*) R. H. Platel and L. L. Schafer, *Chem. Commun.*, 2012, **48**, 10609–10611; (*b*) G. Midya, B. Parasar, K. Dharab and J. Dash, *Org. Biomol. Chem.*, 2014, **12**, 1812; (*c*) S. D. Wobser, C. J. Stephenson, M. Delferro and T. J. Marks, *Organometallics*, 2013, **32**, 1317–1327.

11 H. Wang, M. G. H. Vicente, F. R. Fronczek and K. M. Smith, *Chem. – Eur. J.*, 2014, **20**, 5064–5074.

12 (*a*) N. K. Swamy, L. K. Tatini, J. M. Babu, P. Annamalai and M. Pal, *Chem. Commun.*, 2007, 1035–1037; (*b*) X. Zeng, *Chem. Rev.*, 2013, **113**, 6864–6900.

13 (*a*) U. Mayerhcffer, M. Gsanger, M. Stolte, B. Fimmel and F. Wurthner, *Chem. – Eur. J.*, 2013, **19**, 218–232; (*b*) A. D. Laurent, C. Adamo and D. Jacquemin, *Phys. Chem. Chem. Phys.*, 2014, **16**, 14334–14356.

14 (*a*) B. Dhokale, P. Gautam and R. Misra, *Tetrahedron Lett.*, 2012, **53**, 2352–2354; (*b*) P. Gautam, B. Dhokale, V. Shukla, C. P. Singh, K. S. Bindra and R. Misra, *J. Photochem. Photobiol., A*, 2012, **239**, 24–27; (*c*) R. Misra, P. Gautam, R. Sharma and S. M. Mobin, *Tetrahedron Lett.*, 2013, **54**, 381–383; (*d*) T. Jadhav, R. Maragani, R. Misra, V. Sreeramulu, D. N. Rao and S. M. Mobin, *Dalton Trans.*, 2013, **42**, 4340–4342; (*e*) R. Misra, P. Gautam, T. Jadhav and S. M. Mobin, *J. Org. Chem.*, 2013, **78**, 4940–4948; (*f*) R. Sharma, R. Maragani, S. M. Mobin and R. Misra, *RSC Adv.*, 2013, **3**, 5785; (*g*) R. Misra, T. Jadhav and S. M. Mobin, *Dalton Trans.*, 2013, **42**, 16614–16620; (*h*) R. Maragani and R. Misra, *Tetrahedron Lett.*, 2013, **54**, 5399–5402; (*i*) R. Misra, T. Jadhav and S. M. Mobin, *Dalton Trans.*, 2014, **43**, 2013–2022; (*j*) R. Misra, R. Sharma and S. M. Mobin, *Dalton Trans.*, 2014, **43**, 6891–6896; (*k*) R. Misra, T. Jadhav, B. Dhokale and S. M. Mobin, *Chem. Commun.*, 2014, **50**, 9076–9078; (*l*) V. A. Nadtochenko, N. N. Denisov, V. Y. Gak, N. V. Abramova and N. M. Loim, *Russ. Chem. Bull.*, 1999, **48**, 1900; (*m*) S. Barlow and S. R. Marder, *Chem. Commun.*, 2000, 1555–1562.

